Coded Pattern Unsourced Random Access with Analyses on Sparse Pattern Demapper

Zhentian Zhang, Graduate Student Member, IEEE, Bo An, Student Member, IEEE, Kai-Kit Wong, Fellow, IEEE, Jian Dang, Senior Member, IEEE, Christos Masouros, Fellow, IEEE, Zaichen Zhang, Senior Member, IEEE, and Chan-Byoung Chae, Fellow, IEEE

Abstract—In this paper, we introduce a novel framework for multiple access code design under the finite blocklength regime in multi-input and multi-output (MIMO) systems, termed coded pattern multiple access (CPMA). CPMA involves a series of multiple access code designs facilitated by a sparse pattern mapper/demapper, enabling independent information projection onto transmission patterns. Unlike existing approaches, the mapping and demapping of patterns are completely isolated components, ensuring energy-efficient transmission. In this work, we establish and analyze practical CPMA models, thoroughly investigating the performance limits of a potential non-bijective demapper. Closed-form and integral-form solutions are provided to describe these performance limits. Additionally, we present a practical application of CPMA: the coded pattern unsourced random access (CPURA) scheme. This scheme is designed for finite blocklength transmission under a quasi-static fading channel. The proposed CPURA achieves bound-approaching performance for large user groups, outperforming existing state-of-the-art methods in the context of massive machine-type communications (mMTC). Notably, the minimum required energy-per-bit to support 1.200 active users exhibits only a 1.3 dB gap from the achievable bound, validating the potential of the proposed CPMA framework.

Index Terms—Multi-input and multi-output (MIMO), finite blocklength regime, coded pattern multiple access (CPMA), massive mchine-type communications (mMTC), unsourced random access (URA), coded pattern unsourced random access (CPURA).

I. INTRODUCTION

A. Background And Related Works

Research in the finite blocklength regime, also known as non-asymptotic information theory [1], [2], plays a pivotal role in addressing the emerging challenges in massive access applications [3], such as the Internet of Things (IoT) and massive machine-type communications (mMTC). The design

- Z. Zhang, B. An, J. Dang, Z. Zhang are with the National Mobile Communications Research Laboratory, Frontiers Science Center for Mobile Information Communication and Security, Southeast University, Nanjing, 210096, China. Jian Dang, Zaichen Zhang are also with the Purple Mountain Laboratories, Nanjing 211111, China. (e-mails: {zhangzhentian, anbo, dangjian, zczhang}@seu.edu.cn).
- K.-K. Wong and C. Masouros are with the Department of Electronic and Electrical Engineering, University College London, Torrington Place, WC1E 7JE, United Kingdom and K. K. Wong is also affiliated with Yonsei Frontier Lab, Yonsei University, Seoul, Korea. (e-mails: {kai-kit.wong, c.masouros}@ucl.ac.uk).
- C.-B. Chae is with the School of Integrated Technology, Yonsei University, Seoul 03722, South Korea (e-mail: cbchae@yonsei.ac.kr).

Corresponding authors: J. Dang (dangjian@seu.edu.cn), Z. Zhang (zczhang@seu.edu.cn)

of multiple access codes [5], [6] has a significant impact on the systematic user capacity. Traditional strategies such as ALOHA, coded slotted ALOHA, CDMA, and treating interference as noise (TIN) become less effective as the number of access users increases [4]. However, recent advances in finite blocklength transmission, specifically unsourced random access (URA) and unsourced multiple access (UMA) [7], offer a promising approach for efficiently supporting an unbounded number of users¹. The achievability bound with prior activity information under a Gaussian multiple access channel (GMAC) are elegantly derived in [7], while [9] provides the achievable bound without known activity under GMAC. Additionally, the case of quasi-static fading in GMAC is discussed in [10], and [11] summarizes various practical URA code designs for GMAC.

In practical terms, the finite coherence blocklength refers to the transmission duration during which the channel response remains constant. As discussed in [12], the coherence time is approximated as $1/4D_s$, where D_s represents the maximal Doppler spread. For instance, with a 2 GHz carrier, the channel coherence time ranges from 1 millisecond to 45 milliseconds, depending on the transmitter's speed, which can vary from 3 km/h to 120 km/h. Additionally, the sampling frequency typically falls within the range of 100 kHz to 500 kHz in outdoor environments, aligned with the corresponding coherence bandwidth. Consequently, the finite blocklength is typically in the range of $10^2 \sim 10^4$.

Recent advancements in multi-input, multi-output (MIMO) URA systems [13]–[15] provide valuable benchmarks for designing MIMO-URA schemes under quasi-static MIMO fading channels. Numerous state-of-the-art studies have explored various aspects of MIMO-URA, including sparse codes [16]–[26], random spreading [27], [28], and coupled/uncoupled tree-based methods [12], [29]–[34], among others. A comparison of these approaches in terms of systematic user capacity can be found in [39]. Also, the coding gain from URA has been effectively applied to related research areas, such as integrated sensing and communication (ISAC) [40]–[44] and reconfigurable intelligent surfaces (RIS) [45].

¹URA/UMA refers to a set of techniques enabled by concatenated code design. In URA, users transmit information using a shared common codebook, and the receiver's decoder produces a list of messages without identifying individual users. For more detailed information, a comprehensive survey can be found in [8].

B. Challenges

Despite many promising URA schemes have been invented, there are challenges remaining to be tackled. Specifically, random spreading in URA typically requires carefully designed optimization for power allocation and finite channel usage to accommodate varying user group sizes. Additionally, random spreading relies on non-linear mapping and demapping, which provides robust anti-disturbance capability but incurs prohibitively high computational complexity. For instance, the fading spread unsourced random access (FASURA) [27] achieves favorable performance but requires computational resources on the order of 10^{10} for 300 active users. Similarly, the sparse kronecker product (SKP) coding scheme [28] delivers the good capacity performance, but its parameters need frequent adjustments depending on the user group size. This makes the scalability of random spreading methods impractical for large user groups. In contrast, sparse code-based MIMO-URA schemes offer greater flexibility and can be implemented with tolerable performance losses. For example, the slotted non-orthogonal pilot-based polar code (SNOP-Polar) [20] performs almost identically to SKP for small user groups, and shows a 0.65 dB performance gap at 1,000 users. Notably, URA designs with the on-off division multiple access (ODMA) framework [19], [24], [34], [58] have attracted significant attention recently due to their flexible transmission structure and strong robustness.

Moreover, there remains a significant gap between practical MIMO-URA designs and the achievable capacity. No existing works have fully achieved the achievability bound as anticipated by [15] across both small and large user group sizes, especially as the number of active users exceeds 1,000. One potential reason for this shortcoming is that the current state-of-the-art approaches are primarily based on optimized methods derived from conventional non-orthogonal multiple access schemes, such as interleave division multiple access (IDMA) [35], sparse code multiple access (SCMA) [36], and CDMA. For instance, a direct extension of IDMA, as discussed in [17], exhibits poor performance in the low energy-per-bit region, where satisfying interleaving pattern priors becomes challenging. While it performs well in high energy-per-bit regions, it suffers from significant degradation at lower energy levels. Similarly, the multi-stage orthogonal pilot-based polar code (MSOP-Polar) proposed in [25] effectively mitigates errors arising from pilot collisions through its multi-stage structure. However, the sparse patterns of signals remain dependent on preambles, and if the preamble estimation is inaccurate, decoding failure occurs throughout the entire frame. The overall transmission structure of MSOP-Polar, which mirrors the two-phase transmission model of IDMA, is thus subject to similar decoding drawbacks when the number of active users is large.

C. Contributions

Distinct from existing state-of-the-art approaches, a novel multiple access principle, called coded pattern multiple access (CPMA), is introduced. The applications of CPMA under finite blocklength transmission are then explored, with a practical implementation presented in the form of a coded pattern unsourced random access (CPURA) scheme.

Currently, the patterns of transmitted signals are dependent on previous information, with restoration relying on signals from earlier stages, such as interleaving patterns [35], SCMA codebooks [36], and index modulation patterns [37], [38]. It is important to note that our work differs significantly from the aforementioned fields, where the system operates in a coordinated manner, e.g., user node size for SCMA codebook design and user states for index modulation transmission pattern optimization. Specifically, to control the transmission pattern under prescribed constraints [38], the receiver must be aware of the states of all users. This requirement is unrealistic for mMTC and URA scenarios, as coordinated schemes cannot support an unbounded number of devices [7]. This limitation explains why index modulation-based URA schemes [37] still rely on modulation patterns that are coupled with pilot selection, i.e., if the modulation patterns are independent from pilot selection, the uncoupled structure would allow for additional transmission degree of freedom (DoF) and thus improve the transmission efficiency.

Thus, it is unlikely to transmit abundant information independently without additional overhead such as energy consumption or additional prior constraints when the pattern selection is always dependent on previous information. In other words, the DoF at the encoder side is not fully utilized. However, if the information can be independently projected onto transmission patterns and these patterns can be restored without any prior knowledge, more efficient transmission (energy-wise or redundancy-wise) becomes achievable by conveying messages through the transmission patterns themselves. In summary, to enhance transmission efficiency, all necessary priors, such as pattern sequences in index modulation and constellation location codebooks in SCMA, should be fully independent and unknown at the receiver so that their information-carrying capacity can be further improved.

To this end, the proposed CPMA introduces a *sparse pattern encoder (SPE)*, through which the information of a single user can be projected onto both the transmitted signals (such as phase shift keying (PSK) constellation symbols) and the patterns by which the symbols are permuted. Notably, the projection of source messages is entirely independent of any other encoder components, allowing for detection and estimation at the receiver without the need for any prior knowledge. This approach enables more efficient transmission by ensuring independent mapping and demapping from source messages to patterns.

The main contributions of this paper is listed as follows:

1) Theoretical Analyses on Non-Bijective Demapping in CPMA: The rationale behind CPMA and the SPE, specifically the mapping procedure, is introduced within the context of practical multiple access models under a quasi-static MIMO fading channel. With these models established, we provide both closed-form and integral-form performance limits for the demapping of uncoded CPMA, which involves the joint restoration of transmitted signals and embedded patterns. Numerical results, compared with those from a practical detector, demonstrate the viability and accuracy of our analyses.

- 2) Application under Finite Blocklength with Practical CPMA Design: In addition to the theoretical analysis of abstract multiple access models, we also present a practical CPMA design for MIMO-URA, achieving near-optimal performance of minimum-required energy-per-bit (system metric for user volume capacity) for large group sizes. Both the encoder and decoder designs are aligned with the principles of the proposed CPMA, demonstrating the potential of the newly introduced DoF for multiple access code design under finite blocklength conditions.
- 3) Comparisons with Classic Schemes and Recent Advances under Finite Blocklength: We conduct extensive simulations to compare the proposed CPURA with a variety of multiple access schemes designed for finite blocklength, aiming to showcase the potential superiority of the newly developed CPURA. The results demonstrate that CPURA can achieve near-optimal systematic capacity under unsourced finite blocklength conditions.

The content is organized as follows: Sec. II introduces the rational of CPMA and provides closed-form and integral-form performance limit analyses for the practical models. Sec. III details the application of the proposed CPMA in the design of a practical MIMO-URA scheme, based on the principles of CPMA. Sec. IV presents numerical results comparing both theoretical and empirical solutions. Finally, conclusions are drawn in Sec. V.

Notations: The operations $(\cdot)^T$, $(\cdot)^H$, and $(\cdot)^{-1}$ represent transpose, conjugate transpose and inverse, respectively. $\mathbb{E}[\cdot]$ and $\mathrm{Cov}[\cdot]$ are the expectation and covariance of a random variable. $f(\cdot)$ and $M(\cdot)$ represent the probability density function (PDF) and the moment generating function (MGF). $\mathbb{C}^{N\times M}$ stands for the set of $N\times M$ complex matrices. $|\cdot|$ and $||\cdot||$ are the complex modulus and the spectral norm. $x\sim \mathcal{CN}(a,b)$ denotes the circularly symmetric complex Gaussian random variable with mean a and variance b.

II. CODED PATTERN MULTIPLE ACCESS

In this section, the general rational of CPMA is introduced along with the theoretical analyses on the performance limit of single/multi-user via Maximum Likelihood (ML) detection under quasi-static fading channel. However, ML-based detection costs complexity in the order of $\mathcal{O}\left((Q+1)^{K_a}\right)$, which is prohibitively large and intolerable for massive connectivity. For alternative with reduced complexity, we also introduce how to conduct iterative detection via a near-optimum (near-ML) probabilistic data association (PDA) detector with complexity in the order of $\mathcal{O}(K_a^3)$.

A. Novel Projection Method: Sparse Pattern Encoding (SPE)

Assume B bits (possibly after redundant encoding, e.g., channel coding) are transmitted over L channel uses via a random access code/projection denoted by \mathcal{X} . The binary source $\mathbf{u} \in \{0,1\}^{1 \times B}$ is encoded/projected into a frame \mathbf{x} with sparsity ratio α :

$$\mathcal{X}[\mathbf{u}] \to \mathbf{x} \in \{0, \mathcal{Q}\}^{1 \times L},$$

$$\|\mathbf{x}\|_{0} = \alpha L \ll B, \quad \alpha \in [0, 1],$$
 (1)

where $Q \in \mathbb{C}^{1 \times Q}$ denotes the scaled constellation symbols with modulation order Q, and the L_0 -norm $\|\mathbf{x}\|_0$ equals the number of non-zero elements in the frame. Equation (1) represents a class of *sparse pattern encoding* (SPE) methods that embed information into sparse frame patterns.

The encoded frame follows the power constraint defined by energy-per-bit E_b/N_0 :

$$E_b/N_0 = \frac{E_s L}{\sigma^2 B},\tag{2}$$

where E_s is the energy per channel use and the aggregate power equals E_sL , i.e., $\|\mathbf{x}\|_2^2 = E_sL$.

Compared with the average power of non-sparse modulation $\bar{P}_{\text{non-s}} = \frac{E_s L \log_2 Q}{B}$, sparse encoding yields a magnitude gain for the non-zero elements in \mathbf{x} :

Magnitude Gain =
$$\frac{\bar{P}_{\rm s}}{\bar{P}_{\rm non-s}} = \frac{B}{\alpha L \log_2 Q}$$
, (3)

where the average power of the non-zero elements is $\bar{P}_{\rm s} = \frac{E_s L}{\alpha L}$, while the zero elements consume no power (e.g., idle slots with only background noise). Thus, by constructing a sparse structure when $B \gg \alpha L \log_2 Q$, the transmitted signal power can exceed the average power per B bits.²

According to (3), the proposed CPMA encourages sparse frame construction combined with high-order modulation. Under SPE, the information of B bits is conveyed by both the non-zero symbols and their permutation patterns, i.e., the sparse frame structure. Hence, SPE provides a design framework that achieves robust performance under sparse transmission with high-order modulation.

Notably, with the addition of a zero state from the SPE, the elements in x are no longer mapped in a bijective (one-toone) manner. As a result, the receiver must detect and estimate both the sparse patterns of sub-frames and the transmitted non-zero signals. The following section establishes toy models for both single-user and multi-user cases, explaining the performance limits of probabilistic detection and decoding for each scenario. Special emphasis is placed on the analytical error performance, particularly the symbol error rate (SER). We derive a closed-form solution for the SER in the nonbijective mapping of CPMA. In Sec. III, the SPE concept is integrated into the design of the sparse pattern encoder. This approach embeds a large number of binary bits into sub-frame patterns. By leveraging the additional sparsity DoF, the sparse structure enhances the power levels of transmitted constellation symbols. For a more detailed description, please refer to Sec. III-A.

B. Single/Multi-User Case: Toy Model and Analyses

The matrix $\mathbf{H} \in \mathbb{C}^{N_r \times K_a}$ denotes the channel coefficients between K_a users and the receiver with N_r antennas, and vector $\mathbf{s}_i \in \mathbb{C}^{K_a \times 1}$ denotes the transmitted signals at single slot with $(1+Q)^{K_a}$ potential combinations and $i \in \{1,\ldots,(1+Q)^{K_a}\}$. The received signal at given slot of time can be written as:

$$\mathbf{y} = \mathbf{H}\mathbf{s}_i + \mathbf{n},\tag{4}$$

 2 Here, B denotes the number of bits modulated and transmitted, which may differ from the original source bits before encoding.

where $\mathbf{s}_i = [s_{i_1}, s_{i_2}, \cdots, s_{i_{K_a}}]^\mathrm{T}$, and s_{i_k} dedicated for the k-th user is selected from the constellation set $\{0, \mathcal{Q}\}$ and $\mathbf{n} \sim \mathcal{CN}\left(\mathbf{0}, \sigma^2 \mathbf{I}\right)$ is the additive white Gaussian noise (AWGN) at the receiver.

When the ML detector is applied, the PEP of deciding on $\mathbf{s}_{\hat{i}}$ given that \mathbf{s}_{i} is transmitted is defined as:

$$P(\mathbf{s}_i \to \mathbf{s}_{\hat{i}}) = \mathbb{E}_{\mathbf{H}} \left[\int_{\sqrt{\frac{\Gamma}{2\sigma^2}}}^{\infty} \frac{1}{\sqrt{2\pi}} e^{-\frac{t^2}{2}} dt \right], \tag{5}$$

where $\Gamma \triangleq \|\mathbf{H}(\mathbf{s}_i - \mathbf{s}_{\hat{i}})\|^2$ and $\mathbb{E}_{\mathbf{H}}[\cdot]$ is the expectation with respect to the channel matrix \mathbf{H} . The SER upper-bound is derived as [46], [47]:

$$SER_{ML} \le \sum_{i=1}^{(Q+1)^{K_a}} \sum_{\hat{i}=1, \hat{i} \ne i}^{(Q+1)^{K_a}} \frac{P(\mathbf{s}_i \to \mathbf{s}_{\hat{i}})}{(Q+1)^{K_a}}.$$
 (6)

Furthermore, the unconditional PEP can be rewritten as:

$$P(\mathbf{s}_i \to \mathbf{s}_{\hat{i}}) = \frac{1}{\pi} \int_0^{\pi/2} M_{\Gamma} \left(\frac{-1}{4\sin^2(\eta)\sigma^2} \right) d\eta, \tag{7}$$

where $f_{\Gamma}(\cdot)$ and $M_{\Gamma}(\cdot)$ represent the PDF and the MGF of Γ , respectively. To get the MGF of Γ , the distribution of Γ needs to be analyzed. Let $Z_{n_r,k}+jW_{n_r,k}$ represent the n_r^{th} row and k^{th} column element of the channel matrix \mathbf{H} , where $Z_{n_r,k}$ and $W_{n_r,k} \sim \mathcal{CN}(0,\frac{1}{2})$ are independent identically distributed (iid) Gaussian random variables. The vector $\mathbf{H}(\mathbf{s}_i-\mathbf{s}_{\hat{i}})$ is given by:

$$\mathbf{H}(\mathbf{s}_{i} - \mathbf{s}_{\hat{i}}) = \begin{bmatrix} \sum_{k=1}^{K_{a}} m_{1,k}^{i_{k}} + j \sum_{k=1}^{K_{a}} n_{1,k}^{i_{k}} \\ \vdots \\ \sum_{k=1}^{K_{a}} m_{N_{r},k}^{i_{k}} + j \sum_{k=1}^{K_{a}} n_{N_{r},k}^{i_{k}} \end{bmatrix}, \quad (8)$$

where $m_{n_r,k}^{i_k} = (\Re(s_{i_k}) - \Re(s_{\hat{i}_k}))Z_{n_r,k} - (\Im(s_{i_k}) - \Im(s_{\hat{i}_k}))W_{n_r,k}$, $n_{n_r,k}^{i_k} = (\Re(s_{i_k}) - \Re(s_{\hat{i}_k}))W_{n_r,k} + (\Im(s_{i_k}) - \Im(s_{\hat{i}_k}))Z_{n_r,k}$, and $\Re(\cdot)$ and $\Im(\cdot)$ are the real and imaginary parts of a complex value. Note that $m_{n_r,k}^{i_k}$ and $n_{n_r,k}^{i_k}$ are Gaussian random variables with zero mean and a variance of $\frac{|s_{i_k} - s_{\hat{i}_k}|^2}{2}$. The covariance between $m_{n_r,k}^{i_k}$ and $n_{n_r,k}^{i_k}$ can be expressed as:

$$\begin{split} & \text{Cov}[m_{n_r,k}^{i_k}, n_{n_r,k}^{i_k}] \\ &= \mathbb{E}[m_{n_r,k}^{i_k} n_{n_r,k}^{i_k}] - \mathbb{E}[m_{n_r,k}^{i_k}] \mathbb{E}[n_{n_r,k}^{i_k}] \\ &= \left(\Re(s_{i_k}) - \Re(s_{\hat{i}_k})\right) \left(\Im(s_{i_k}) - \Im(s_{\hat{i}_k})\right) \left(\mathbb{E}[Z_{n_r,k}^2] - \mathbb{E}[W_{n_r,k}^2]\right) \\ &= 0. \end{split}$$

Based on the characteristics of Gaussian random variables, $m_{n_r,k}^{i_k}$ and $n_{n_r,k}^{i_k}$ are iid Gaussian random variables. Let $M_{n_r} = \sum_{k=1}^{K_a} m_{n_r,k}^{i_k}$ and $N_{n_r} = \sum_{k=1}^{K_a} n_{n_r,k}^{i_k}$. It is derived that M_{n_r} and N_{n_r} are iid Gaussian random variables with zero mean and a variance of $\frac{\|\mathbf{s}_i - \mathbf{s}_i\|^2}{2}$. Thus, Γ is given by:

$$\Gamma = \sum_{r_{n}=1}^{N_{r}} M_{n_{r}}^{2} + \sum_{r_{n}=1}^{N_{r}} N_{n_{r}}^{2}.$$
 (10)

From (10), Γ follows a generalized central chi-square distribution with a degree of freedom of $2N_r$. Therefore, the unconditional PEP is given by:

$$P(\mathbf{s}_i \to \mathbf{s}_{\hat{i}}) = \frac{1}{\pi} \int_0^{\pi/2} \left(1 + \frac{\|\mathbf{s}_i - \mathbf{s}_{\hat{i}}\|^2}{4\sin^2(\eta)\sigma^2} \right)^{-N_r} d\eta. \tag{11}$$

Furthermore, $P(\mathbf{s}_i \rightarrow \mathbf{s}_i)$ is upper-bounded by:

$$P(s_i \to s_{\hat{i}}) \le \frac{1}{2} \left(1 + \frac{\|\mathbf{s}_i - \mathbf{s}_{\hat{i}}\|^2}{4\sigma^2} \right)^{-N_r}.$$
 (12)

Eventually, the upper bound of the SER is expressed as:

 $SER_{ML} \leq$

$$\frac{1}{2} \sum_{i=1}^{(Q+1)^{K_a}} \sum_{\hat{i}=1, \hat{i} \neq i}^{(Q+1)^{K_a}} \frac{1}{(Q+1)^{K_a}} \left(1 + \frac{\|\mathbf{s}_i - \mathbf{s}_{\hat{i}}\|^2}{4\sigma^2}\right)^{-N_r}.$$
(13)

C. Probabilistic Data Association (PDA) Detector

In this section, we present a practical estimator that offers much lower complexity than the ML detector while incurring only marginal performance loss. Similar ideas have been employed in various schemes [21], [22], [34]. Specifically, the received signal from $K_a \geq 1$ users at a given time slot is expressed as:

$$\mathbf{y} = \mathbf{h}_k \underbrace{s_i}_{\text{Target Symbol}} + \underbrace{\sum_{j \neq i}^{K_a} \mathbf{h}_k s_j}_{} + \mathbf{n}, \quad (14)$$

Intra-UE Interference Terms

which can be written into a more compact form:

$$y = Hs + n. (15)$$

After channel equalizer such as zero forcing (ZF), (15) can be rewritten as:

$$\tilde{\mathbf{y}} = \mathbf{s} + \tilde{\mathbf{n}}.\tag{16}$$

where $\tilde{\mathbf{y}} = (\mathbf{H}^{\mathrm{H}}\mathbf{H})^{-1}\mathbf{H}^{\mathrm{H}}\mathbf{y}$ and $\tilde{\mathbf{n}}$ is the Gaussian noise with zero mean and covariance matrix $\mathbf{\Lambda} = \sigma^2 (\mathbf{H}^{\mathrm{H}}\mathbf{H})^{-1}$. PDA detector aims to calculate the a posteriori probabilities (APPs) corresponding to all potential symbols, i.e., the goal is to calculate $p(s_i | \mathbf{y}), s_i \in \{0, Q\}$.

Define $\mathbf{e}_j = [0, 0, \dots, 1, \dots]^T$ as a K_a -length indicator vector with only one non-zero element at the j-th position. (16) can be rewritten as:

$$\tilde{\mathbf{y}} = \underbrace{s_i \mathbf{e}_i}_{\text{Target}} + \underbrace{\sum_{j \neq i} s_j \mathbf{e}_j + \tilde{\mathbf{n}}}_{\text{Pseudo Noise } \tilde{\mathbf{N}}}.$$
(17)

To update the target's APPs of potential symbols in set $\{0, \mathcal{Q}\}$, pseudo noise $\tilde{\mathbf{N}}_k$ is treated as a Gaussian distributed noise with:

Mean
$$\mathbf{E}_i = \sum_{j \neq i} \bar{s}_j \mathbf{e}_j$$
,

Covariance $\Omega_i = \sum_{j \neq i} \omega_j \mathbf{e}_j \mathbf{e}_j^{\mathrm{T}} + \mathbf{\Lambda}$, (18)

Pseudo Covariance $\mathbf{\Xi}_i = \sum_{j \neq i} \xi_j \mathbf{e}_j \mathbf{e}_j^{\mathrm{T}}$,

where the intermediate variables $\bar{s}_j, \omega_j, \xi_j$ are calculated by:

$$\bar{s}_{j} = \sum_{s_{j} \in \{0, \mathcal{Q}\}} s_{j} p(s_{j} | \mathbf{y}),$$

$$\omega_{j} = \sum_{s_{j} \in \{0, \mathcal{Q}\}} (s_{j} - \bar{s}_{j})(s_{j} - \bar{s}_{j})^{*} p(s_{j} | \mathbf{y}),$$

$$\xi_{j} = \sum_{s_{j} \in \{0, \mathcal{Q}\}} (s_{j} - \bar{s}_{j})(s_{j} - \bar{s}_{j}) p(s_{j} | \mathbf{y}).$$

$$(19)$$

The APP $p(s_j|\mathbf{y}), s_j \in \{0, Q\}$ initialization starts as a uniform distribution. To update APPs, set $\mathbf{w} = \tilde{\mathbf{y}} - s_i \mathbf{e}_i - \mathbf{E}_i$ and

$$\mathbf{\Phi}(s_i) = \exp\left(-\begin{pmatrix} \Re(\mathbf{w}) \\ \Im(\mathbf{w}) \end{pmatrix}^{\mathrm{T}} \mathbf{\Lambda}_i \begin{pmatrix} \Im(\mathbf{w}) \\ \Re(\mathbf{w}) \end{pmatrix}\right),$$

$$\mathbf{\Lambda}_i = \begin{pmatrix} \Re(\mathbf{\Omega}_i + \mathbf{\Xi}_i) & \Im(\mathbf{\Xi}_i - \mathbf{\Omega}_i) \\ \Im(\mathbf{\Omega}_i + \mathbf{\Xi}_i) & \Re(\mathbf{\Omega}_i - \mathbf{\Xi}_i) \end{pmatrix}^{-1}.$$
(20)

The APP update can be achieved, combined with (14)-(20):

$$p(s_i|\mathbf{y}) = \frac{\mathbf{\Phi}(s_i)}{\sum_{s_i \in \{0, Q\}} \mathbf{\Phi}(s_i)}.$$
 (21)

By iteration, the APPs of all users' transmitted signals with respect to the potential symbols in the constellation table are estimated.

III. APPLICATION: MASSIVE MIMO CODED PATTERN UNSOURCED RANDOM ACCESS

As an application of the novel CPMA, we introduce a practical CPMA scheme and apply it to the recently proposed unsourced random access problem [7] in the context of a massive MIMO receiver. The proposed coded pattern unsourced random access (CPURA) scheme achieves user capacity close to the theoretical limit [15], following the principles of sparse pattern encoding. A practical sparse pattern encoder³ is introduced, utilizing a two-phase concatenated code and slotted transmission structure. The encoder and decoder designs are shared across all transmission chunks.

The channel model follows quasi-static Rayleigh fading, identical to Sec. II, where a fixed but unknown number K_a of users transmit B bits of information over L channel uses. Let $\mathbf{u}_k \in \{0,1\}^{B\times 1}$ and $\mathbf{g}_k \in \mathbb{C}^{1\times M}$ denote the message vector and channel coefficient vector of the k-th user, respectively. The message set is denoted by \mathcal{L} , i.e., $\mathbf{u}_k \in \{\mathcal{L}\}$. All users employ the proposed two-phase concatenated code with slotted transmission across J_s chunks, consisting of a pilot signal (PS) phase and a permuted data (PD) phase, occupying L_p and L_c channel uses, respectively, such that $L/J_s = L_p + L_c$. The receiver decodes the superimposed signals to produce a candidate message list $\tilde{\mathcal{L}}$.

The single-user power constraint is expressed by the energy-per-bit E_b/N_0 in (2). The system performance is measured by the per-user probability of error (PUPE), which accounts for both missed detections and false alarms, defined as:

$$P_{\mathrm{md}} = \frac{\mathbb{E}[n_{\mathrm{md}}]}{K_a}, P_{\mathrm{fa}} = \mathbb{E}\left[\frac{n_{\mathrm{fa}}}{|\tilde{\mathcal{L}}|}\right],$$
 (22)

³The sparse pattern encoder in this paper represents a viable design approach in line with the proposed coded pattern multiple access. The design is not restricted to the structure presented in this paper.

where the number of transmitted but not detected messages equals to $n_{\rm md}$ and the number of never transmitted but detected as valid is denoted by $n_{\rm fa}$. For the URA problem under quasi-static fading, the goal is to minimize the minimum-required energy-per-bit E_b/N_0 to reach a PUPE target $P_{e,\rm trg}$. The spectral efficiency (SE) is denoted by $\mu=B/L$. The following will introduce the proposed sparse pattern encoder (SPER) and its employment in CPURA and more importantly we also analyze the error probability of the proposed CPURA.

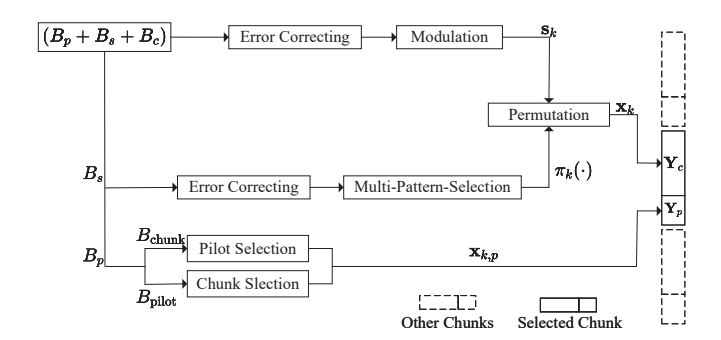


Fig. 1. Proposed encoder design for single user.

A. Sparse Pattern Encoder (SPER) for CPURA

The proposed sparse pattern encoder (SPER) provides a general framework and is not restricted to the specific structure introduced here. It comprises three main components: pilot selection, coded pattern selection, and modulation with permutation. Notably, pattern selection is independent of pilot selection and is also randomized. The encoded messages are generated from a randomized binary source. Accordingly, the binary bits are partitioned into three segments, B_p , B_s , and B_c , such that $B = B_p + B_s + B_c$. The overall encoder design is illustrated in Fig. 1.

1) Slotted Transmission and Pilot Selection: The first B_p bits are further divided into $B_{\rm chunk}$ and $B_{\rm pilot}$ bits., i.e., $B_p = B_{\rm chunk} + B_{\rm pilot}$. The whole transmission period is divided into $J_s = 2^{B_{\rm chunk}}$ chunks and each user selects which chunk to transmit signals by the decimal integer of the $B_{\rm chunk}$ bits. Moreover, let $\mathbf{A} = [\mathbf{a}_1, \mathbf{a}_2, \dots, \mathbf{a}_{N_p}] \in \mathbb{C}^{L_p \times N_p}, N_p = 2^{B_{\rm pilot}}$ denote the common pilot codebook where the codeword follows the power constraint of $\|\mathbf{a}_i\|_2^2 = \beta E_s L, i \in [1:N_p]$ and ratio β determines the power allocated to the PS phase. By the decimal integer of the $B_{\rm pilot}$ bits, each user select the pilot codeword with the corresponding index and transmit the signal over L_p -length channel uses. We use $\mathbf{x}_{k,p}$ to denote the pilot signal of the k-th user. Therefore, at given transmission chunk, the overlapped pilot signals $\mathbf{Y}_p \in \mathbb{C}^{L_p \times N_r}$ can be written as:

$$\mathbf{Y}_p = \sum_k \mathbf{x}_{k,p} \mathbf{g}_k + \mathbf{N}_p, \tag{23}$$

where $\mathbf{N}_p \sim \mathcal{CN}\left(\mathbf{0}, \sigma^2 \mathbf{I}\right)$ is the AWGN with zero mean and σ^2 variance.

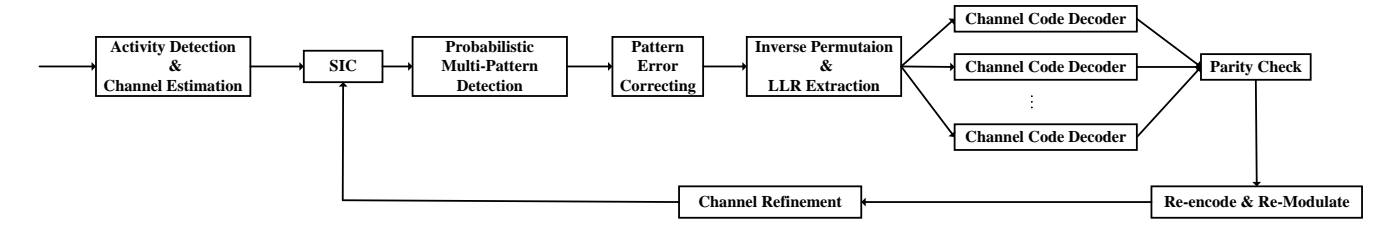


Fig. 2. Proposed decoder design where SIC refers to successive interference cancellation.

2) Coded Pattern Selection: After pilot selection, each user chooses and encodes multiple permutation patterns by B_s bits. Firstly, the B_s bits are encoded with channel code into E bits. Then, the channel coded pattern bits are then segmented into J_p segments to select J_p patterns. Let $\mathbf{P} \in \{0,1\}^{\frac{L_c}{J_p} \times N_c}, N_c = 2^{\frac{E}{J_p}}$ denote the common pattern codebook where each codeword has only αL_c non-zero elements indicating the position for constellation symbol transmission. All J_p pattern codewords construct the sparse pattern of the whole PD frame. We use $\pi_k(\cdot)$ to denote the permutation maneuver by the selected patterns of the k-th user. For example, with pattern codeword [1,0,1,0,0,1], one can do the following permutation:

$$\underbrace{\begin{bmatrix} s_1 \\ s_2 \\ s_3 \end{bmatrix}}_{\text{Vector } \mathbf{x}} \xrightarrow{\pi_k(\cdot)} \underbrace{\pi_k(\mathbf{x}) = \begin{bmatrix} s_3 \\ 0 \\ s_1 \\ 0 \\ 0 \\ s_2 \end{bmatrix}}, \tag{24}$$

where the permutation can be arbitrary and there are adequate permutation resources, e.g., for a duration with 38 channel uses, if one wish to select 4 active positions for signal transmission and others idle, there are $\binom{38}{4} = 73815$ different combinations. The codebook **P** is generated with N_c unique pattern codewords so that each pattern codeword can carry information of $\log_2 N_c$ bits.

3) Modulation and Permutation: After selection of pilot and patterns, the rest B_c bits are first encoded by FEC code with R_c code rate and then modulated with Q modulation order. We use vector $\mathbf{s}_k \in \mathbb{C}^{\frac{B_c}{\log_2 QR_c} \times 1}$ to denote the FEC-encoded and modulated vector with power constraint $\|\mathbf{s}_k\|_2^2 = (1-\beta)E_sL$. Thereupon, the transmitted signals at the PD phase $\mathbf{Y}_c \in \mathbb{C}^{L_c \times N_r}$ can be written as:

$$\mathbf{Y}_{c} = \sum_{k} \pi_{k}(\mathbf{s}_{k})\mathbf{g}_{k} + \mathbf{N}_{c},$$

$$= \sum_{k} \mathbf{x}_{k}\mathbf{g}_{k} + \mathbf{N}_{c},$$
(25)

where $\mathbf{x}_k = \pi_k(\mathbf{s}_k) \in \mathbb{C}^{L_c \times 1}$ denotes the signal of sparse frame with permuted constellation symbols.

B. Sparse Pattern Decoder (SPDR) for CPURA

Since the transmission during each chunk is independent, all received signals share identical procedures of the following sparse pattern decoder (SPDR) design. The SPDR consists of three major components, namely activity detection and channel estimation (ADCE), probabilistic multi-pattern detection (PMPD) and successive interference cancellation (SIC). We use $\mathbf{Y} = [\mathbf{Y}_p; \mathbf{Y}_c] \in \mathbb{C}^{\frac{L}{J_s} \times N_r}$ to denote the received signal at single chunk. The proposed decoder design is summarized in Fig. 2.

1) Activity Detection and Channel Estimation (ADCE): Initially, the receiver aims to estimate the number of active users at single chunk, which can be realized by exploiting the power information of the received signal Y:

$$K_{\text{est}} = \left\lfloor \frac{1}{E_s L} \left(\frac{\|\mathbf{Y}\|_F^2}{N_r} - \sigma^2 (L_c + L_p) \right) \right\rfloor. \tag{26}$$

After power detection, we treat signal in PS phase (23) as a sparse recovery problem which has been studied rigorously [49]–[52]. For convenience, we employ simultaneous orthogonal matching pursuit (SOMP) [53] to perform ADCE. SOMP is a greedy algorithm with an iterative workflow. In each iteration, it matches the codeword with the largest correlation to the residual signal and estimates the corresponding channel vector for the matched codeword. After the matching and estimation process, the algorithm updates the residual signal through orthogonal projection. Finally, with AD results, the linear equalizer of minimum mean square error (MMSE) is adopted to estimate the channel vectors of the codewords verdicted to be active.

The Moore-Penrose Inverse dominates the complexity around $\mathcal{O}(N_r L_p N_p)$ which can be reduced to $\mathcal{O}(N_r N_p \log N_p)$ if sub-sampled discrete Fourier Transformation (DFT) matrix is adopted and the matrix multiplication is replaced by Fast Fourier Transformation (FFT) [18].

2) Probabilistic Multi-Pattern Detection (PMPD): With the estimated channel vectors, one can proceed the decoding on signals at PD phase (25) via the PDA detector. With PDA detector, one can obtain the probabilistic information towards all states in set $\{0,\mathcal{Q}\}$, i.e., APPs. Let vector $\tilde{\mathbf{x}}_k\left((j-1)\cdot\frac{L_c}{J_p}+1,j\cdot\frac{L_c}{J_p}\right)\in\mathbb{C}^{\frac{L_c}{J_p}\times 1}$ denote the estimated j-th sub-frame at the PD phase where the value of elements in $\tilde{\mathbf{x}}_j,j\in[1:J_p]$ equals to the APP of active state, i.e., the summation of all the APPs of constellation symbols. The decoder multiplies the active state APPs of elements in vector $\tilde{\mathbf{x}}_j$ at the non-zero location in pattern codebook \mathbf{P} to calculate the joint activity probability $P_{\rm activity}$:

$$P_{\text{act},n_c} = \prod_{k \in \mathcal{A}_{n_c}} \tilde{\mathbf{x}}_j(k), k \in [1:\frac{L_c}{J_p}], n_c \in [1:N_c], \quad (27)$$

where set \mathcal{A}_{n_c} has the index location of all non-zero elements in the n_c pattern codeword in codebook \mathbf{P} . Segment by segment, all activity probability P_{act,n_c} of J_p patterns of the frame at PD phase are restored. The joint activity probability will be utilized to generate soft information for error correcting decoding on the encoded pattern bits.

3) Non-Linear/Linear Demodulation and Log-Likelihood Extraction: The projection of pattern bits into a pattern codeword evidently belongs to non-linear modulation and thus we conduct non-linear demodulation as follows to extract the log-likelihood ratio (LLR) of the pattern bits to conduct error correcting decoding. The LLR of the n-th, $n \in [1:\frac{B_s}{J_p}]$ bit within a pattern segment can be calculated by:

$$LLR_{n} = \ln \frac{P_{\text{act},n_{c}}(b_{n} = 0|\mathbf{Y_{c}})}{P_{\text{act},n_{c}}(b_{n} = 1|\mathbf{Y_{c}})}$$

$$= \ln \frac{\sum_{\mathbf{b}_{\sim n}} P_{\text{act},n_{c}}(b_{n} = 0|\mathbf{Y_{c}})\Pi_{i\neq n}P(b_{i})}{\sum_{\mathbf{b}_{\sim n}} P_{\text{act},n_{c}}(b_{n} = 1|\mathbf{Y_{c}})\Pi_{i\neq n}P(b_{i})},$$
(28)

where $\mathbf{b}_{\sim n} = \{b_1, \dots, b_{n-1}, b_{n+1}, \dots\}$ denotes the binary expansion of the integer of segment index excluding b_n and $\Pi_{i\neq n}P(b_i)$ equals the prior probability multiplication of elements in $\mathbf{b}_{\sim n}$. The non-linear demodulation on single segment bit requires N_c times of search to calculate the marginal probabilities, thereby the overall demodulation complexity scales as $\mathcal{O}(EN_c)$. After error correcting code on pattern bits, parity check is conducted to validate the detected pattern sequences. With all the verified patterns, the decoder inversely permutes the frame to extract transmitted constellation symbols, denoted by $\pi^{-1}(\cdot)$. The complexity of finding the possible patterns scales as $\mathcal{O}(J_p N_p)$. Then, with APPs towards all constellation symbols, the LLR information of bits are calculated for the subsequent channel code decoding, e.g., there are information of two bits carried by a constellation symbol in quadrature phase shift keying (QPSK), i.e., $[b_0, b_1] \rightarrow s_{b_0, b_1}$. Thereupon, the LLRs of b_0 and b_1 can be obtained respectively by:

LLR₀ = ln
$$\frac{p(s_{0,0}|\mathbf{y}) + p(s_{0,1}|\mathbf{y})}{p(s_{1,0}|\mathbf{y}) + p(s_{1,1}|\mathbf{y})},$$

LLR₁ = ln $\frac{p(s_{0,0}|\mathbf{y}) + p(s_{1,0}|\mathbf{y})}{p(s_{0,1}|\mathbf{y}) + p(s_{1,1}|\mathbf{y})}.$ (29)

4) Successive Interference Cancellation (SIC): After channel code decoding, the decoder conducts parity check to determine the correctness of the produced binary message, e.g., for low density parity check code (LDPC), the parity check is often done with the generator matrix; For Polar code, one can achieve robust check with cyclic redundancy check (CRC) bits. We use $\mathbf{X}_{\mathrm{SIC}}$ to denote the re-encoded and re-modulated signals (including signals at both PS and PD phases) of all the parity-check-passed messages at current SIC iteration. Subsequently, the receiver refines the channel estimation with longer observations [27] by:

$$\mathbf{G}_{\mathrm{SIC}} = \left(\mathbf{X}_{\mathrm{SIC}}^{\mathrm{H}} \mathbf{X}_{\mathrm{SIC}} + \sigma^{2} \mathbf{I}\right)^{-1} \mathbf{X}_{\mathrm{SIC}}^{\mathrm{H}} \mathbf{Y}.$$
 (30)

Then, the decoder subtracts the restored signals from the original one for the next SIC round by $Y-Y_{\rm SIC}$ where $Y_{\rm SIC}=X_{\rm SIC}G_{\rm SIC}$.

TABLE I
PARAMETER SETUPS OF FIG. 3 AND FIG. 4

Single User Case, Fig. 3	
Definition	Parameter
Frame Length	$L = 10^4$
Bits Num	B = 100
Frame Sparsity	$\alpha \in \{0.01, 0.005, 0.001\}$
Antenna Num	$N_r \in \{5, 10\}$
PSK Order	$Q \in \{2, 4\}$
Multi-User Case, Fig. 4	
Definition	Parameter
User Num	$K_a = 4$
Antenna Num	$N_r = 10$
Frame Sparsity	$\alpha = 0.001$

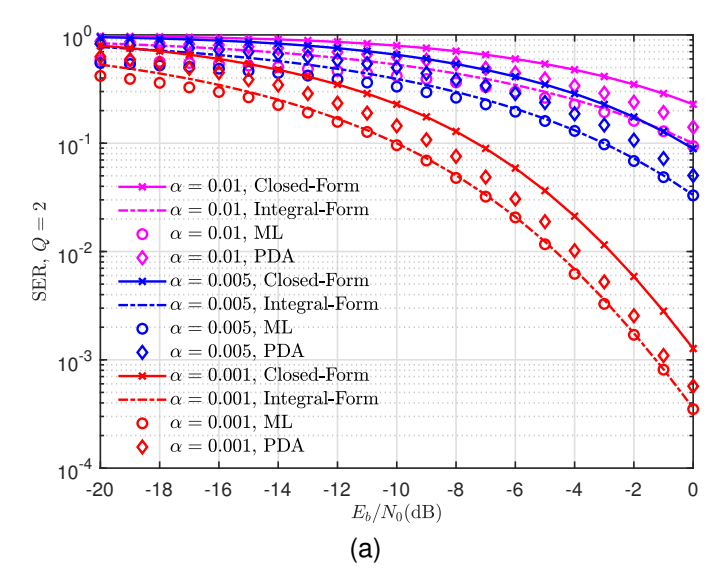
IV. NUMERICAL RESULTS

In this section, we illustrate the proposed CPMA under various setups to show the potential from the newly developed sparsity DoF. Particularly, we emphasize on the comparisons with the recent advances in multiple access design for finite blocklength catering to the application scenarios for future communication networks. For choice of common pilot codebook, we generate pilot codebook via sub-sampled DFT matrix for the proposed CPURA in the sequel. The pattern codewords are randomly and uniquely generated by the required sparsity without any further optimization⁴.

1) Non-Bijective Demapping Performance: By comparing the results of empirical ML and PDA, we first demonstrate the accuracy of the integral-form (11) and closed-form (13) solution for symbol error rate (SER) analyses under single user case and multi-user case. The parameter setups are as follows: Assuming each user occupies a $L=10^4$ length frame for B=100 bits transmission where the messages are encoded with a potential SPE encoder and the sparsity of frame equals to $\alpha \in \{0.01, 0.005, 0.001\}$. There are $N_r \in \{5, 10\}$ antennas at the receiver. For set $\{0, Q\}$, sub-set Q contains scaled BPSK constellation symbols for Q=2 and scaled QPSK symbols for Q=4. The probability priors of different statements are initialized with uniform likelihood, i.e., $\frac{1}{Q+1}$. The parameter setups of Fig. 3 and Fig. 4 are summarized in Table I.

Fig. 3 illustrates the non-bijective demapping performance of single user case under different frame sparsity $\alpha \in \{0.01, 0.005, 0.001\}$ and $N_r = 5$ antennas. By different frame sparsity, the transmitted signals will have different power level, i.e., the sparser the frame, the higher the magnitude can be. Consequently, the demapping performance becomes better with lower SER, which can be observed under both Q = 2 and Q = 4. Meanwhile, there is a SER loss between the ML detector and the PDA detector, around 10% performance loss with PDA but saving 50% and 75% of the computational complexity at single user case with Q = 2 and Q = 4 respectively. Therefore, PDA detector can be a good alternative for ML

⁴Optimizing pattern codewords may be beneficial for interference reduction, capacity improvement, etc. However, this work primarily focuses on enabling sparse pattern encoding and decoding. Interestingly, collisions among pattern codewords have minimal impact on performance, as they can be effectively separated and decoded from noisy observations when user channel coefficients are independent.



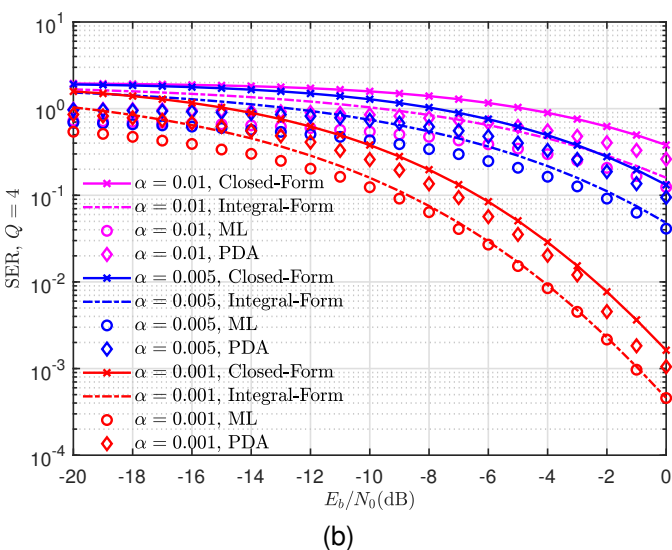


Fig. 3. Non-bijective demapping performance of the empirical and theoretical results of single user case under $B=100,\,L=10^4,\,N_r=5$ under different frame sparsity α and different modulation order: a) Performance comparisons under BPSK, Q=2; b) Performance comparisons under QPSK, Q=4.

detector for non-bijective demapping. Furthermore, one can observe good performance matches between the ML detector and the integral-form solution, especially at the moderate and higher energy-per-bit region. Also, the performance of PDA distributes between the predicted performance of closed-form and integral form results. The aforementioned results indicate the correctness of our analyses, i.e., the provided integral-form SER can predict the non-bijective demapping well and the closed-form SER offers good SER upperbound prediction.

Fig. 4 illustrates the non-bijective demapping performance under multi-user case with $K_a=4,\ N_r=10$ and $\alpha=0.001.$ Similar to the single user case, common results can be found. The empirical performance by ML detector is well-predicted by the integral-form solution. The PDA detector has slightly worse performance compared with ML detector at the low energy-per-bit $E_b/N_0({\rm dB})$ region but indistinguishable performance to ML at the moderate and high energy-per-bit

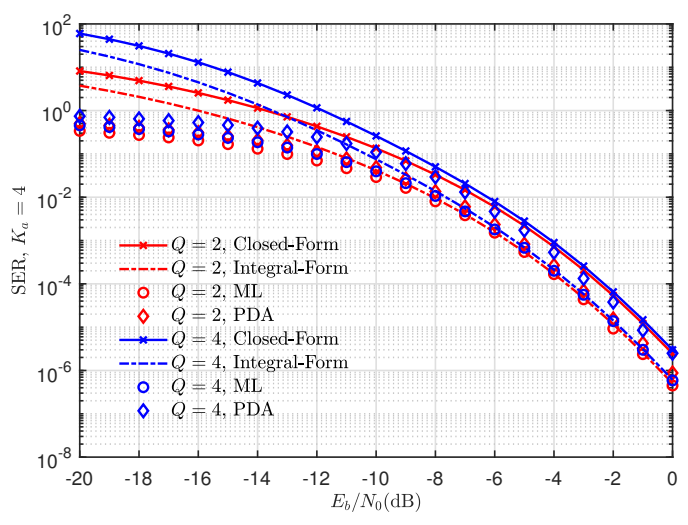


Fig. 4. Non-bijective demapping performance of multi-user case with $K_a=4$, $N_r=10$ and $\alpha=0.001$ under different modulation order Q+1.

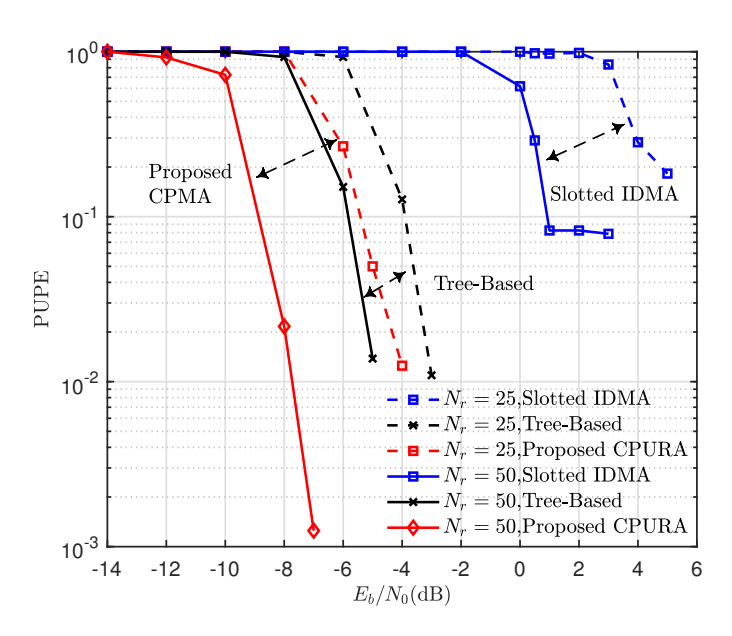


Fig. 5. Performance compared with classic multiple access codes including IDMA [17] and Tree-Based approach [30] under different energy-per-bit with $K_a=64$ and $N_r\in\{25,50\}$.

region. More importantly, the computational complexity of PDA detector has much slower rising speed than ML under increased number of active users K_a .

Overall, for the potential non-bijective demapping of the novel CPMA, we have offered solid performance analyses for both single user case and multi-user case. The spirit of PDA detector indeed can be utilized for practical CPMA decoder design, since it has near-ML multi-user detection performance and rather smaller instrument complexity.

2) Performance Compared With Classic Multiple Access: Since the spirit of IDMA [35] and tree-based [30] have been adopted in many relevant areas, this subsection compares the proposed CPMA with IDMA and tree-based scheme. For equity, the proposed practical CPMA is compared with slotted version of [17], which can be quite feasible and straightfor-

TABLE II
PARAMETER SETUPS OF
THE SLOTTED IDMA AND THE PROPOSED CPURA

$ \begin{array}{ c c c c } \hline \text{Definition} & \text{Parameter} \\ \hline \text{Channel Uses} & L = 3200 \\ \hline \text{Bits Num} & B = 100 \\ \hline \text{Spectral Efficiency (SE)} & \mu = 0.03125 \\ \hline \text{PSK Order} & Q = 4 \text{, QPSK} \\ \hline \text{Channel Code} & 256\text{-LDPC} \\ \hline \text{Pilot Codebook Size} & 2^{10} \\ \hline \text{Pilot Length} & 31 \\ \hline \text{Transmission Chunk Num} & 2^4 \\ \hline \text{Channel Estimation Iteration} & 15 \\ \hline \text{Proposed CPURA Parameter Setups} \\ \hline \hline \text{Definition} & \text{Parameter} \\ \hline \text{Info Bits} & B = 1683 \\ \hline \text{Channel Uses} & L = 53856 \\ \hline \text{Spectral Efficiency (SE)} & \mu = 0.03125 \\ \hline \text{Pilot Length} & B_{\text{pilot}} = 14 \\ \hline \text{Chunk Bits} & B_{\text{chunk}} = 5 \\ \hline \text{Bits To Be Polar Code} & B_{c} = 832 \\ \hline \text{Pattern Bits (before channel coding)} & B_{s} = 832 \\ \hline \text{Sub-Pattern Num (after channel coding)} & B_{s} = 832 \\ \hline \text{Sub-Pattern Non-Zero Num} & 8 \\ \hline \text{Error Correcting Code} & 1024\text{-Polar Code} \\ \hline \text{CR Code} & 24\text{-CRC} \\ \hline \text{Decoding List Size} & 256 \\ \hline \text{Power Allocation Ratio} & \beta = 0.1 \\ \hline \text{Tree-Based approach: CRC-BMST Parameter Setups} \\ \hline \text{Definition} & \text{Parameter} \\ \hline \text{Info Bits} & B = 75 \\ \hline \text{Channel Uses} & L = 2400 \\ \hline \text{CR Clouk Num} & 11 \\ \hline \text{Pilot Bits} & B_{p} = 15 \\ \hline \text{Memory Depth} & 6 \\ \hline \end{array}$			
$\begin{array}{c ccccccccccccccccccccccccccccccccccc$	Slotted IDMA Parameter Setups		
$\begin{array}{c ccccccccccccccccccccccccccccccccccc$			
$\begin{array}{c ccccccccccccccccccccccccccccccccccc$	Channel Uses	L = 3200	
$\begin{array}{c ccccccccccccccccccccccccccccccccccc$	Bits Num		
$\begin{array}{c ccccc} \text{Channel Code} & 256\text{-LDPC} \\ \text{Pilot Codebook Size} & 2^{10} \\ \text{Pilot Length} & 31 \\ \text{Transmission Chunk Num} & 2^4 \\ \text{Channel Estimation Iteration} & 30 \\ \text{Multi-User Detection Iteration} & 15 \\ \hline & \text{Proposed CPURA Parameter Setups} \\ \hline & \text{Definition} & \text{Parameter} \\ \hline & \text{Info Bits} & B = 1683 \\ \text{Channel Uses} & L = 53856 \\ \text{Spectral Efficiency (SE)} & \mu = 0.03125 \\ \text{Pilot Bits} & B_{\text{pilot}} = 14 \\ \text{Pilot Length} & L_p = 467 \\ \text{Chunk Bits} & B_{\text{chunk}} = 5 \\ \text{Bits To Be Polar Code} & B_c = 832 \\ \text{Pattern Bits (before channel coding)} & B_s = 832 \\ \text{Sub-Pattern Num (after channel coding)} & J_p = 64 \\ \text{Sub-Pattern Length} & 19 \\ \text{Pattern Codebook Size} & 2^{16} \\ \text{Sub-Pattern Non-Zero Num} & 8 \\ \text{Error Correcting Code} & 1024\text{-Polar Code} \\ \text{CRC Code} & 24\text{-CRC} \\ \text{Decoding List Size} & 256 \\ \text{Power Allocation Ratio} & \beta = 0.1 \\ \text{PDA Iteration} & 15 \\ \hline & \text{Tree-Based approach: CRC-BMST Parameter Setups} \\ \hline & \text{Definition} & \text{Parameter} \\ \text{Info Bits} & B = 75 \\ \text{Channel Uses} & L = 2400 \\ \text{Spectral Efficiency (SE)} & \mu = 0.03125 \\ \text{Chunk Num} & 11 \\ \text{Pilot Bits} & B_p = 15 \\ \hline \end{array}$	Spectral Efficiency (SE)	$\mu = 0.03125$	
$\begin{array}{c ccccccccccccccccccccccccccccccccccc$	PSK Order		
$\begin{array}{c ccccccccccccccccccccccccccccccccccc$	Channel Code		
$\begin{array}{c ccccccccccccccccccccccccccccccccccc$	Pilot Codebook Size	2^{10}	
$\begin{array}{c ccccccccccccccccccccccccccccccccccc$	Pilot Length		
$\begin{array}{c ccccccccccccccccccccccccccccccccccc$	Transmission Chunk Num	2^4	
$\begin{array}{c ccccccccccccccccccccccccccccccccccc$	Channel Estimation Iteration	30	
$\begin{array}{c ccccccccccccccccccccccccccccccccccc$	Multi-User Detection Iteration	15	
$\begin{array}{c ccccccccccccccccccccccccccccccccccc$	Proposed CPURA Parameter Setups		
$\begin{array}{c c} \text{Channel Uses} \\ \text{Spectral Efficiency (SE)} \\ \text{Pilot Bits} \\ \text{Pilot Length} \\ \text{Chunk Bits} \\ \text{Bits To Be Polar Code} \\ \text{Pattern Bits (before channel coding)} \\ \text{Sub-Pattern Num (after channel coding)} \\ \text{Pattern Codebook Size} \\ \text{Sub-Pattern Length} \\ \text{Pattern Non-Zero Num} \\ \text{Error Correcting Code} \\ \text{CRC Code} \\ \text{Decoding List Size} \\ \text{Power Allocation Ratio} \\ \text{PDA Iteration} \\ \text{Tree-Based approach: CRC-BMST Parameter Setups} \\ \text{Spectral Efficiency (SE)} \\ \text{Chunk Num} \\ \text{Pilot Bits} \\ \text{P} = 15 \\ \end{array}$	Definition		
$\begin{array}{c ccccccccccccccccccccccccccccccccccc$	Info Bits	B = 1683	
$\begin{array}{c ccccccccccccccccccccccccccccccccccc$	Channel Uses	L = 53856	
$\begin{array}{c ccccccccccccccccccccccccccccccccccc$	Spectral Efficiency (SE)	$\mu = 0.03125$	
$\begin{array}{c ccccccccccccccccccccccccccccccccccc$	Pilot Bits	$B_{\rm pilot} = 14$	
Bits To Be Polar Code Pattern Bits (before channel coding) Sub-Pattern Num (after channel coding) Pattern Codebook Size Sub-Pattern Length Pattern Non-Zero Num Error Correcting Code CRC Code Decoding List Size Power Allocation Ratio PDA Iteration Tree-Based approach: CRC-BMST Parameter Setups Definition Info Bits Channel Uses Spectral Efficiency (SE) Chunk Num Pilot Bits $B_c = 832$ $B_s = 832$ $J_p = 64$ 2 ¹⁶ 19 19 24-CRC 24-CRC 24-CRC 256 $\beta = 0.1$ 15 Parameter Setups Parameter Setups Definition Info Bits $B = 75$ $L = 2400$ $\mu = 0.03125$	Pilot Length		
Pattern Bits (before channel coding) $B_s = 832$ $J_p = 64$ 2^{16} Sub-Pattern Codebook Size $Sub-Pattern Length$ Pattern Non-Zero Num $Error Correcting Code \\ CRC Code \\ Decoding List Size Power Allocation Ratio \\ PDA Iteration \\ PDA Iteration \\ Info Bits \\ Channel Uses \\ Spectral Efficiency (SE) \\ Chunk Num \\ Pilot Bits \\ B = 832 J_p = 64 2^{16} 19 19 40 40 40 40 40 40 40 40$	Chunk Bits	$B_{\rm chunk} = 5$	
$\begin{array}{c ccccccccccccccccccccccccccccccccccc$	Bits To Be Polar Code	$B_c = 832$	
Pattern Codebook Size Sub-Pattern Length Pattern Non-Zero Num Error Correcting Code CRC Code Decoding List Size Power Allocation Ratio PDA Iteration Tree-Based approach: CRC-BMST Parameter Setups Definition Info Bits Channel Uses Spectral Efficiency (SE) Chunk Num Pilot Bits $D = \frac{2^{16}}{19}$ $\frac{2^{16}}{19}$ $\frac{2^{16}}{10}$ $\frac{2^{10}}{10}$ $$	Pattern Bits (before channel coding)	$B_s = 832$	
$\begin{array}{c ccccccccccccccccccccccccccccccccccc$	Sub-Pattern Num (after channel coding)		
$\begin{array}{c ccccccccccccccccccccccccccccccccccc$	Pattern Codebook Size	2^{16}	
$ \begin{array}{c ccccccccccccccccccccccccccccccccccc$	Sub-Pattern Length	19	
$ \begin{array}{c cccc} \text{CRC Code} & 24\text{-CRC} \\ \text{Decoding List Size} & 256 \\ \text{Power Allocation Ratio} & \beta = 0.1 \\ \text{PDA Iteration} & 15 \\ \hline \text{Tree-Based approach: CRC-BMST Parameter Setups} \\ \hline & & & & & & & \\ \hline & & & & & & \\ \hline & & & &$	Pattern Non-Zero Num	8	
$\begin{array}{c cccc} \text{Decoding List Size} & 256 \\ \text{Power Allocation Ratio} & \beta = 0.1 \\ \text{PDA Iteration} & 15 \\ \hline \\ \hline \textbf{Tree-Based approach: CRC-BMST Parameter Setups} \\ \hline \textbf{Definition} & \textbf{Parameter} \\ \textbf{Info Bits} & B = 75 \\ \textbf{Channel Uses} & L = 2400 \\ \textbf{Spectral Efficiency (SE)} & \mu = 0.03125 \\ \textbf{Chunk Num} & 11 \\ \textbf{Pilot Bits} & B_p = 15 \\ \hline \end{array}$	Error Correcting Code	1024-Polar Code	
$\begin{array}{c ccccc} \text{Power Allocation Ratio} & \beta = 0.1 \\ \hline \text{PDA Iteration} & 15 \\ \hline \\ \text{Tree-Based approach: CRC-BMST Parameter Setups} \\ \hline & Definition & Parameter \\ Info Bits & B = 75 \\ Channel Uses & L = 2400 \\ Spectral Efficiency (SE) & \mu = 0.03125 \\ Chunk Num & 11 \\ Pilot Bits & B_p = 15 \\ \hline \end{array}$	CRC Code	24-CRC	
$ \begin{array}{ c c c c c c } \hline & PDA & Iteration & 15 \\ \hline \hline & Tree-Based & approach: CRC-BMST & Parameter & Setups \\ \hline & Definition & Parameter \\ & Info & Bits & B = 75 \\ & Channel & Uses & L = 2400 \\ & Spectral & Efficiency & SE) & \mu = 0.03125 \\ & Chunk & Num & 11 \\ & Pilot & Bits & B_p = 15 \\ \hline \end{array} $	Decoding List Size	256	
	Power Allocation Ratio	$\beta = 0.1$	
$\begin{array}{c cccc} & \text{Definition} & \text{Parameter} \\ & \text{Info Bits} & B = 75 \\ & \text{Channel Uses} & L = 2400 \\ & \text{Spectral Efficiency (SE)} & \mu = 0.03125 \\ & \text{Chunk Num} & 11 \\ & \text{Pilot Bits} & B_p = 15 \\ \end{array}$	PDA Iteration	15	
$\begin{array}{c} \text{Info Bits} \\ \text{Channel Uses} \\ \text{Spectral Efficiency (SE)} \\ \text{Chunk Num} \\ \text{Pilot Bits} \end{array} \begin{array}{c} B = 75 \\ L = 2400 \\ \mu = 0.03125 \\ 11 \\ B_p = 15 \end{array}$	Tree-Based approach: CRC-BMST Parameter Setups		
$\begin{array}{c} \text{Channel Uses} \\ \text{Spectral Efficiency (SE)} \\ \text{Chunk Num} \\ \text{Pilot Bits} \end{array} \begin{array}{c} L = 2400 \\ \mu = 0.03125 \\ 11 \\ B_p = 15 \end{array}$	Definition	Parameter	
$\begin{array}{ccc} \text{Spectral Efficiency (SE)} & \mu = 0.03125 \\ \text{Chunk Num} & 11 \\ \text{Pilot Bits} & B_p = 15 \end{array}$	Info Bits	B = 75	
$ \begin{array}{c c} \text{Chunk Num} & 11 \\ \text{Pilot Bits} & B_p = 15 \end{array} $	Channel Uses	L = 2400	
Pilot Bits $B_p = 15$	Spectral Efficiency (SE)	$\mu = 0.03125$	
- p c	Chunk Num	11	
	Pilot Bits	$B_p = 15$	
	Memory Depth		

TABLE III
CRC POLYNOMIALS FOR TREE ENCODER/DECODER IN CRC-BMST

CRC Code	Polynomial of the CRC Bits Generator
6-CRC	$x^6 + x^2 + x + 1$
8-CRC	$x^8 + x^7 + x^6 + x^4 + x^2 + x + 1$
9-CRC	$x^9 + x^6 + x^5 + x^4 + x^3 + 1$
14-CRC	$x^{14} + x^{10} + x^9 + x^7 + x^6 + x^5 + x + 1$

Note: The profile of the CRC parity check bits for CRC-BMST [30] is [0,6,8,8,9,9,9,9,9,14] with J=11.

ward. The universal parameter setups are listed below: For IDMA, the channel uses and the number of binary bits are fixed to L=3200 and B=100 bits, i.e., the SE equals to $\mu=100/3200=0.03125$. For the proposed CPURA, the parameter setups are B=1683, L=53856, $B_{\rm pilot}=14$, $B_{\rm chunk}=5$, i.e., 32 transmission chunks, $B_c=832$, $B_s=832$, $J_p=64$, $N_c=2^{16}$, $L_c=1216$, $L_p=467$ and there are 8 non-zero elements in each 19-length pattern codeword. For all phases, Polar code with 1024 length and 24-CRC is utilized as channel code. The list size of Polar code decoder equals to 256. The generator polynomial of 24-CRC is

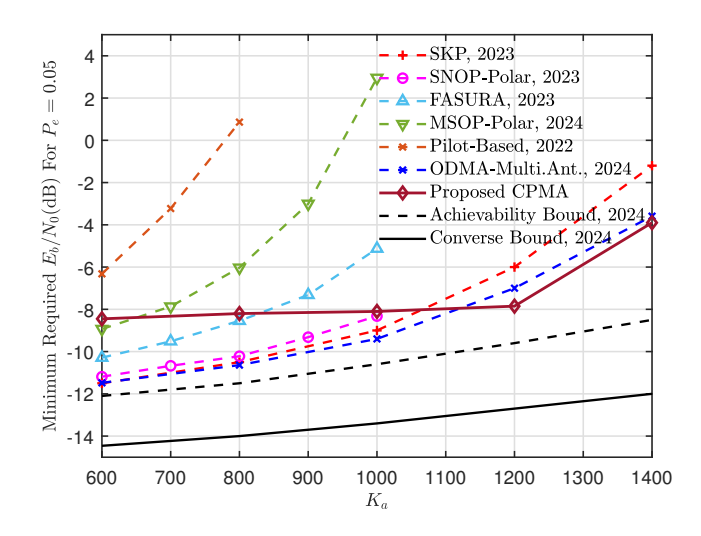


Fig. 6. Performance compared with recent advances under SE=0.03125: a) Capacity performance comparisons under finite blocklength with SE of 0.03125 and $N_r=50$ with benchmarks [18], [20], [25], [27], [28], [58] and Achievable/Converse Bounds in finite blocklength information theory [15].

 $x^{24}+x^{23}+x^{21}+x^{20}+x^{17}+x^{15}+x^{13}+x^{12}+x^8+x^4+x^2+x+1$ and QPSK is adopted for constellation modulation throughout. The power allocation ratio to pilot phase is fixed to $\beta=0.1$. For the tree-encoder/decoder, cyclic redundancy check-based block Markov superposition transmission (CRC-BMST) code is utilized with the same compressive sensing decoder of the proposed scheme. It transmits B=75 information bits with L=2400 channel uses and the memory depth of the BMST is fixed to 6. The parameter setups of slotted IDMA, the proposed CPURA and the CRC-BMST have been summarized in Table III. The tree-based encoder and decoder require parity check allocation which is summarized at Table III.

Fig. 5 illustrates the PUPE performance of classic IDMA, tree-based and the proposed CPURA under different energyper-bit $E_b/N_0(dB)$ with number of active user $K_a=64$ and different number of receiving antennas $N_r \in \{25, 50\}$. Interestingly, all schemes shows a water-falling PUPE drop after an energy-per-bit threshold, e.g., with $N_r=50,\ E_b/N_0=$ -10 dB for the proposed CPURA, $E_b/N_0 = -8 dB$ for the tree-based and $E_b/N_0 = -2 dB$ for the slotted IDMA. The increased number of receiving antenna provides enhanced estimation precision and thus enhance the performance. Meanwhile, an error floor is observed due to the limited codebook size. As shown in Tab. II, slotted IDMA simulations utilize only 1024 pilot codewords, leading to an error floor driven by pilot collision errors, as derived in [39, Eq.34]. In contrast, CPURA, with a codebook size of 214, exhibits a negligible collision error floor of approximately 6.1×10^{-5} under $K_a = 64$. What's more, it is not advisable to simply enlarge the codebook size of slotted IDMA since it will undermines the sub-sampling ratio of the sensing matrix (the codebook) under fixed pilot length, leading to further performance deterioration. Overall, compared with classic multiple access schemes, the proposed scheme in the spirit of CPMA has a promising performance with many desirable features including lower E_b/N_0 threshold and better performance.

3) System Capacity Compared With Recent Advances Under Finite Blocklength Multiple Access: In this subsection, we compare the system capacity between the proposed CPURA and the recent advances under finite blocklength multiple access including practical schemes and the theoretical Achievable/Converse Bounds from finite blocklength information theory [15]. The abbreviations of the benchmarks are superimposed pilot ODMA (SP-ODMA) [24], ODMA with multiple antennas (ODMA-Muti.Ant.) [58], FASURA [27], the SKP coding scheme [28], pilot-based with Polar code (Pilot-Based) [18], SNOP-Polar [20], MSOP-Polar [25]. All works share identical SE of $\frac{100}{3200} = 0.03125$. For any further details on parameter setups of the benchmarks, please refer to the corresponding references.

Fig. 6 illustrates the minimum required energy-per-bit to achieve the target PUPE of 0.05 for different number of active users $K_a \in [600:1400]$ under identical SE of 0.03125 and $N_r = 50$. Notably, there is only a 1.3dB gap between the proposed CPURA and the achievable bound at $K_a = 1200$. Interestingly, the tendency of the CPURA curve has a very low inertia compared with others, which is caused by the high order non-linear demodulation⁵, i.e., pattern segments bits projected to N_c potential patterns. The demodulation can not produce qualified LLR without certain level of energy-per-bit. While many existing works fail when $K_a \geq 1000$, the proposed CPURA scheme demonstrates improved capacity performance compared with some of the best state-of-the-arts, including ODMA-Multi.Ant. and SKP.

This bound-approaching capacity at $K_a=1200$ under finite blocklength can be attributed to the much enhanced averaged power level of the transmitted signals via the CPMA spirit. Specifically, for the proposed CPMA, there are B=1683 binary bits but only 512 QPSK constellation symbols are transmitted into the channel while others are embedded into the transmission patterns of the frame including chunk selection and the multiple sub-patterns. According to (3), the magnitude gain scales around $\frac{1295-10}{512\cdot\log_2 Q}\approx 2.495,\ Q=4.$ Yet, the existing work does not poss such magnitude gain feature. For example, SKP transmits 90 bits by 45 QPSK, i.e., by (3), the magnitude gain ratio equals to $\frac{90}{45\cdot\log_2 Q}=1,\ Q=4.$ Consequently, the proposed CPURA has nearly $\frac{2.495}{1}=2.495$ times higher the averaged power level of transmitted signals. Higher averaged power level guarantees robust anti-disturbance capability of the system and thus generates desirable system capacity with the blessing from the proposed CPMA spirit.

Fig. 7 illustrates the complexity comparisons between different schemes. FASURA has the highest complexity and Slotted IDMA has the lowest complexity. Specifically, in terms of the computational complexity of the proposed CPURA, the complexity of single iteration is dominated by ADCE $\mathcal{O}(N_rN_p\log N_p)$, PMPD $\mathcal{O}(K_{\mathrm{est}}^3+J_pN_p)$, i.e., the proposed CPURA consumes complexity around $\mathcal{O}(N_rN_p\log N_p+(\frac{K_a}{J_s})^3+J_pN_p+EN_c)$ with $\mathbb{E}(K_{\mathrm{est}})=\frac{K_a}{J_s}$. For IDMA, the aggregate complexity for single iteration scales as $\mathcal{O}(2\frac{K_a}{J_c}(N_r+1)^2)$

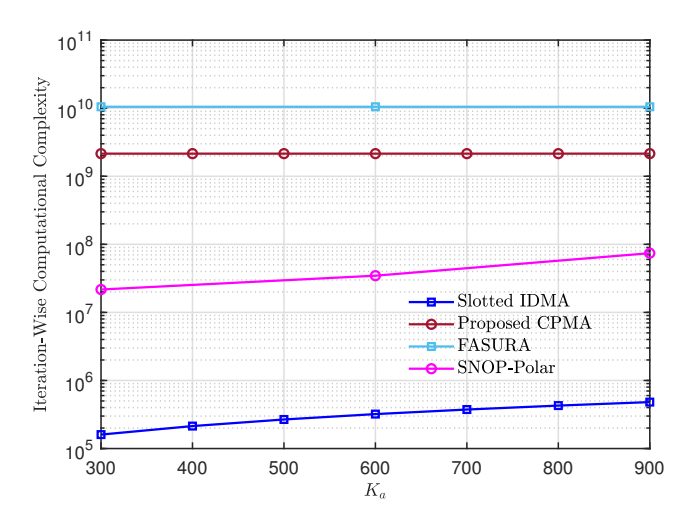


Fig. 7. Iteration-wise computational complexity comparisons between slotted IDMA [17], FASURA [27] and SNOP-Polar [20].

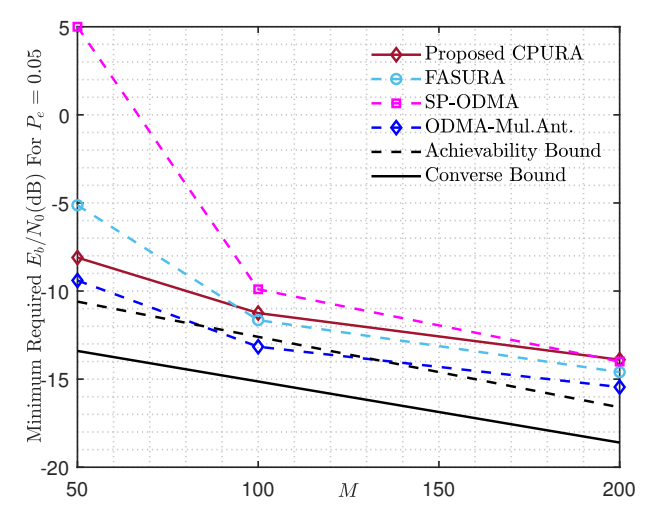


Fig. 8. Minimum required energy-per-bit for $P_e=0.05$ with FASURA [27], SP-ODMA [24], ODMA-Mul.Ant. [58] under different number of receiving antenna $N_r \in \{50, 100, 200\}$ with 1000 active users.

 $1)L_p + \frac{K_a}{J_s}N_rL_c$) whose analyses can be found in [17]. For SNOP-Polar and FASURA, the complexity analyses can be found in [20].

In Fig. 8, the minimum required E_b/N_0 (dB) for 1,000 users is compared with FASURA, SP-ODMA, ODMA-Mul.Ant., and the achievability/converse bounds under different numbers of receiving antennas. At $N_r=50$, the proposed CPURA outperforms FASURA and SP-ODMA by about 3 dB and more than 10 dB, respectively, while being only 1 dB behind the latest ODMA scheme reported in [58]. Moreover, the performance of SP-ODMA and FASURA is more sensitive to the observation dimensions than that of ODMA-Mul.Ant. and CPURA. However, Fig. 6 has illustrated the advantages of the proposed CPMA structures, especially in the high-user regime.

4) SIC Convergence Behavior: In this subsection, we investigate the convergence behavior of the proposed CPURA. Fig. 9 illustrates the PUPE performance of the proposed scheme under varying upper bounds of SIC rounds, with

⁵We have to note that the proposed CPURA concatenated code in spirit of the CPMA is only one realization among many other potential ones

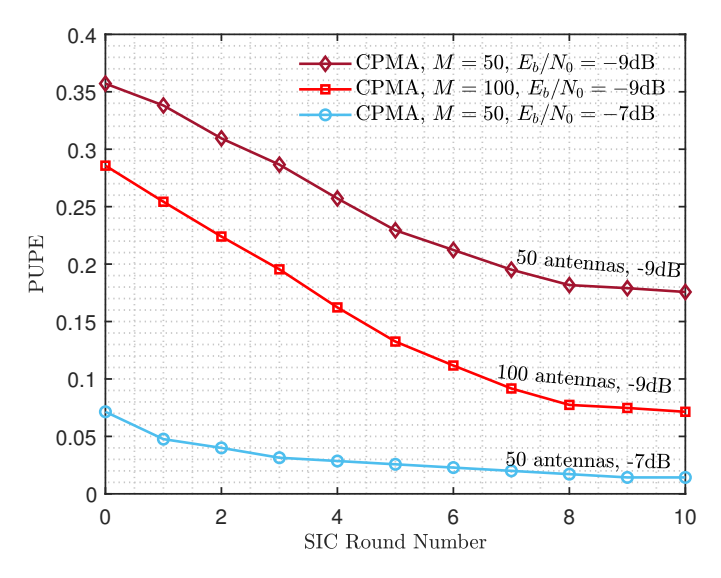


Fig. 9. SIC convergence behavior with 200 active users, receiving antenna $N_r \in \{50,100\}$ and energy-per-bit $E_b/N_0 \in \{-9\text{dB},-7\text{dB}\}$ under different SIC round upperbounds.

200 active users, different numbers of receiving antennas $N_r \in \{50,100\}$, and energy-per-bit levels $E_b/N_0 \in \{-9\,\mathrm{dB},-7\,\mathrm{dB}\}$. No SIC if the round number equals to 0. As predicting the exact number of SIC rounds required for decoding is infeasible, a maximum SIC round limit is set to evaluate convergence across different configurations. The results indicate that SIC convergence is primarily influenced by transmission power. When fixing E_b/N_0 at $-9\,\mathrm{dB}$ and doubling the number of receiving antennas, the final PUPE performance improves, but the convergence speed remains largely unchanged due to the fixed interference level. Conversely, when fixing the number of receiving antennas at 50 and increasing the transmission power, both PUPE performance and convergence speed improve significantly.

5) Remaining Challenges and Promising Solutions: In this subsection, we aims to offer insights into addressing practical implementation challenges in CPURA and propose potential solutions to guide future research directions. The current CPURA design includes key receiver components, such as PMPD (described in Sec. III-B2) and non-linear demodulation (detailed in Sec. III-B3), which focuses on extracting soft bit information from pattern codeword demapping.

Firstly, the complexity of sparse pattern decoding remains to be further reduced for efficient hardware implementations. PMPD, critical to this process, relies on algorithms like ML and PDA, as discussed in Sec. II. Although complexity has been substantially reduced, it remains cubic with respect to activity. Fortunately, advanced algorithm designs offer promising solutions. For instance, [19, Fig.2, Fig.3] introduces a multi-pattern detector based on approximate message passing, achieving linear complexity, which is also explored for MIMO-URA applications. Moreover, the exploitation on favorable channel model structures under particular scenarios remains scarcely discussed, e.g., in [59], each antenna in a massive MIMO channel can be modeled using a spherical wavefront approach, with promising potential for massive MIMO tech-

nology to reduce costs and enhance throughput.

Secondly, the effectiveness of non-linear demodulation as a fundamental solution depends on the channel code employed. In this work, non-linear demodulation, as described by (28), computes the LLR of pattern bits using marginal probabilities, which is necessary for binary-based channel codes like Polar or LDPC codes. However, for advanced channel codes designed for finite blocklength, such as non-binary LDPC [54], [55], this approach can be simplified. With non-binary channel codes, PMPD with efficient algorithms can directly calculate LLRs from non-binary symbol constellation APPs, eliminating additional processing steps. Recent advances in information theory, as highlighted in [56], [57], underscore the promising potential of non-binary channel codes for future applications.

V. CONCLUSIONS

In this work, a novel DoF for multiple access code design is introduced through the proposed CPMA. CPMA generalizes a series of potential code designs that enable independent information mapping on transmitted signals and their permutation patterns. Practical multiple access models for both single-user and multi-user scenarios are established and analyzed. Closed-form and integral-form performance limits are provided. Furthermore, a practical CPURA is elaborated, featuring concatenated encoder/decoder designs with boundapproaching systematic capacity for large group sizes under the finite blocklength regime, specifically in the context of machine-type massive connectivity. Numerical results demonstrate the viability and accuracy of the anticipated performance limits. The performance of the proposed CPURA is compared with various state-of-the-art models, illustrating the superiority of the proposed CPURA. Future work will focus on error frame rate analyses for the proposed CPMA and will explore effective methods for pattern demodulation with higher orders.

ACKNOWLEDGMENT

Z. Zhang would like to thank M. Ozates, the first author of ODMA-Mul.Ant. [58], and M. Hao, the first author of SP-ODMA [24], for the valuable discussions and for providing the data used in Fig. 6 and Fig. 8 for comparison.

REFERENCES

- [1] Y. Polyanskiy, et al., "Channel codingrate in the finite blocklength regime," *IEEE Trans. Inf. Theory*, vol.56, no.5, pp.2307–2359, May 2010.
- [2] P. Mary, et al., "Finite blocklength information theory: What is the practical impact on wireless communications?", in Proc. IEEE GLOBECOM Workshops, pp. 1-6, Dec. 2016.
- [3] X. Chen, et al., "Massive access for 5G and beyond," IEEE J. Sel. Areas Commun., vol. 39, no. 3, pp. 615-637, Mar. 2021.
- [4] Y. Wu, et al., "Massive access for future wireless communication systems," IEEE Wireless Commun., vol. 27, no. 4, pp. 148-156, Aug. 2020.
- [5] N. H. Mahmood, et al., "Machine type communications: Key drivers and enablers towards the 6G era", EURASIP J. Wireless Commun. Netw., vol. 2021, no. 1, pp. 1-25, Dec. 2021.
- [6] Y.-W. Huang and P. Moulin, "Finite blocklength coding for multiple access channels", in *Proc. IEEE Int. Symp. Inf. Theory (ISIT)*, pp. 831-835. Jul. 2012.
- [7] Y. Polyanskiy, "A perspective on massive random-access," in *Proc. IEEE Int. Symp. Inf. Theory (ISIT)*, Aachen, Germany, pp. 2523-2527, Jun. 2017.

- [8] M. Ozates, et al., "Unsourced random access: A comprehensive survey", arXiv preprint, arXiv:2409.14911, 2024.
- [9] K.-H. Ngo, et al., "Unsourced multiple access with random user activity," IEEE Trans. Inf. Theory, vol. 69, no. 7, pp. 4537–4558, Jul. 2023.
- [10] S. S. Kowshik, et al., "Energy efficient random access for the quasistatic fading MAC", in Proc. IEEE Int. Symp. Inf. Theory (ISIT), pp. 2768-2772, Jul. 2019.
- [11] Y. Li, et al., "Unsourced multiple access for 6G massive machine type communications," China Commun., vol. 19, no. 3, pp. 70-87, Mar. 2022.
- [12] A. Fengler, et al., "Non-bayesian activity detection, large-scale fading coefficient estimation, and unsourced random access with a massive MIMO receiver," *IEEE Trans. Inf. Theory*, vol. 67, no. 5, pp. 2925-2951, May 2021.
- [13] Z. Zhang, et al., "On fundamental limits of slow-fluid antenna multiple access for unsourced random access," *IEEE Wireless Commun. Lett.*, Early Access, doi: 10.1109/LWC.2025.3594112.
- [14] J. Gao, et al., "Energy efficiency of MIMO massive unsourced random access with finite blocklength," *IEEE Wireless Commun. Lett.*, vol. 12, no. 4, pp. 743-747, Apr. 2023.
- [15] J. Gao, et al., "Unsourced random access in MIMO quasi-static rayleigh fading channels with finite blocklength" in Proc. IEEE Int. Symp. Inf. Theory (ISIT), Athens, Greece, 2024, pp. 3213-3218.
- [16] Z. Zhang, et al., "Pilot-free unsourced random access via dictionary learning and error-correcting codes," *IEEE Trans. Wireless Commun.*, vol. 23, no. 7, pp. 7488-7502, July 2024.
- [17] T. Li, et al., "Joint device detection, channel estimation, and data decoding with collision resolution for MIMO massive unsourced random access," *IEEE J. Sel. Areas Commun.*, vol. 40, no. 5, pp. 1535-1555, May 2022.
- [18] A. Fengler, et al., "Pilot-based unsourced random access with a massive MIMO receiver, interference cancellation, and power control," *IEEE J. Sel. Areas Commun.*, vol. 40, no. 5, pp. 1522–1534, May 2022.
- [19] Z. Zhang, et al., "Probabilistic ODMA receiver with low-complexity algorithm for MIMO unsourced random access," *IEEE Trans. Veh. Technol.*, Early Access, doi:10.1109/TVT.2025.3570708.
- [20] M. Ozates, et al., "A slotted pilot-based unsourced random access scheme with a multiple-antenna receiver," IEEE Trans. Wireless Commun., Aug. 2023.
- [21] Z. Zhang, et al., "LIM-URA: A less-is-more strategy for quasi-static fading unsourced random access," in Proc. IEEE Wireless Commun. Network. Conf. (WCNC), Milan, Italy, 2025, pp. 1-6.
- [22] Z. Zhang, et al., "Unsourced random access under quasi-static fading channel: A less-is-more strategy," IEEE Trans. Wireless Commun., Early Access, doi: 10.1109/TWC.2025.3603032.
- [23] Z. Zhang, et al., "Sparse code transceiver design for unsourced random access with analytical power division in gaussian MAC," VTC-FALL 2025, Accepted, available: arXiv:2505.01988.
- [24] M. Hao, et al., "Superimposed pilot ODMA transmission for massive MIMO unsourced random access," *IEEE Commun. Lett*, vol. 29, no. 2, pp. 333-337, Feb. 2025.
- [25] M. J. Ahmadi, et al., "Unsourced random access using multiple stages of orthogonal pilots: MIMO and single-antenna structures," *IEEE Trans. Wireless Commun.*, vol. 23, no. 2, pp. 1343-1355, Feb. 2024.
- [26] Z. Zhang, et al., "Unsourced random access via random dictionary learning with pilot-free transceiver design," *IEEE Trans. Wireless Commun.*, vol. 23, no. 12, pp. 17884-17898, Dec. 2024.
- [27] M. Gkagkos, et al., "FASURA: A scheme for quasi-static fading unsourced random access channels," *IEEE Trans. Commun.*, vol. 71, no. 11, pp. 6391-6401, Nov. 2023.
- [28] Z. Han, et al., "Receiver design for MIMO unsourced random access with SKP coding," *IEEE Wireless Commun. Lett.*, vol. 12, no. 1, pp. 45-49, Jan. 2023.
- [29] V. Shyianov, et al., "Massive unsourced random access based on uncoupled compressive sensing: Another blessing of massive MIMO," IEEE J. Sel. Areas Commun., vol. 39, no. 3, pp. 820-834, Mar. 2021.
- [30] H. Cao, et al., "CRC-aided sparse regression codes for unsourced random access," *IEEE Commun. Lett.*, vol. 27, no. 8, pp. 1944-1948, Aug. 2023.
- [31] J. Liu and X. Wang, "Sparsity-exploiting blind receiver algorithms for unsourced multiple access in MIMO and massive MIMO channels," *IEEE Trans. Commun.*, vol. 69, no. 12, pp. 8055-8067, Dec. 2021.
- [32] Z. Zhang, et al., "Uncoupled unsourced random access: Exploiting geographical diversity of access points," *IEEE Trans. Veh. Technol.*, vol. 74, no. 6, pp. 9882-9887, June 2025.
- [33] Z. Zhang, et al., "Unsourced random access with uncoupled compressive sensing and forward error correction," *IEEE Trans. Veh. Technol.*, vol. 74, no. 2, pp. 3555-3560, Feb. 2025.

- [34] Z. Zhang, et al., "Efficient ODMA for unsourced random access in MIMO and hybrid massive MIMO," *IEEE Internet Things J.*, vol. 11, no. 23, pp. 38846-38860, 1 Dec.1, 2024.
- [35] Li Ping, et al., "Interleave division multiple-access," IEEE Wireless Trans. Commun., vol. 5, no. 4, pp. 938-947, Apr. 2006.
- [36] S. Zhang, et al., "Sparse code multiple access: An energy efficient uplink approach for 5G wireless systems", in Proc. IEEE Global Commun. Conf. (GLOBALCOM), pp. 4782-4787, Dec. 2014.
- [37] Y. Su and J. Zheng, "Index modulation multiple access for unsourced random access," *IEEE Wireless Commun. Lett.*, vol. 12, no. 5, pp. 794-798, May 2023.
- [38] C. Wang, et al., "Near-ML low-complexity detection for generalized spatial modulation," *IEEE Commun. Lett*, vol. 20, no. 3, pp. 618-621, Mar. 2016.
- [39] Z. Zhang, et al., "Unsourced random access via random scattering with turbo probabilistic data association detector and treating collision as interference," *IEEE Wireless Trans. Commun.*, vol. 23, no. 12, pp. 17899-17914, Dec. 2024.
- [40] M. J. Ahmadi, et al., "Integrated sensing and communications for unsourced random access: Fundamental limits," in Proc. IEEE Global Commun. Conf. (GLOBALCOM), Cape Town, South Africa, 2024, pp. 1365-1370.
- [41] Q. Zhang, et al., "Joint power allocation and discrete phase-shift optimization for SIM-aided ISAC systems," IEEE Trans. Veh. Technol., doi: 10.1109/TVT.2025.3584064, 2025.
- [42] Q. Dan, et al., "Beamforming for secure RSMA-aided ISAC systems," IEEE Trans. Cogn. Commun. Netw., Early Access doi: 10.1109/TCCN. 2025.3587100, 2025.
- [43] M. J. Ahmadi, et al., "A practical framework for unsourced integrated sensing and communication," in Proc. IEEE SPAWC, Surrey, United Kingdom, 2025, pp. 1-5.
- [44] Z. Zhang, et al., "On fundamental limits for fluid antenna-assisted integrated sensing and communications for unsourced random access", IEEE J. Sel. Areas Commun. Early Access, doi: 10.1109/JSAC.2025.3608113
- [45] M. J. Ahmadi, et al., "RIS-aided unsourced multiple access (RISUMA): Coding strategy and performance limits," *IEEE Wireless Trans. Commun.*, vol. 24, no. 7, pp. 6225-6239, July 2025.
- [46] J. G. Proakis and M. Salehi, "Digital communications," *Digital Communications*, vol. 73, no. 11, pp. 3–5, 2015.
- [47] J. Jeganathan, et al., "Generalized space shift keying modulation for MIMO channels," in Proc. IEEE Int. Symp. Pers. Indoor Mobile Radio Commun. (PIMRC), Sept. 2008, pp. 1–5.
- [48] B. An, et al., "Enhanced reconfigurable intelligent surface-assisted spatial index modulation," *IEEE Trans. Commun.*, vol. 72, no. 5, pp. 2610–2624, May 2024.
- [49] M. Ke, et al., "Compressive sensing-based adaptive active user detection and channel estimation: Massive access meets massive MIMO," IEEE Trans. Signal Process., vol. 68, pp. 764-779, Jan. 2020.
- [50] L. Liu and W. Yu, "Massive connectivity with massive MIMO—Part I: Device activity detection and channel estimation," *IEEE Trans. Signal Process.*, vol. 66, no. 11, pp. 2933–2946, Jun. 2018.
- [51] S. Jiang, et al., "EM-AMP-based joint active user detection and channel estimation in cell-free system," *IEEE Syst. J.*, vol. 17, no. 3, pp. 4026-4037, Sept. 2023.
- [52] Z. Gao, et al., "Compressive-sensing-based grant-free massive access for 6G massive communication," *IEEE Internet Things J.*, vol. 11, no. 5, pp. 7411-7435, 1 Mar. 2024.
- [53] J. -F. Determe, et al., "On the exact recovery condition of simultaneous orthogonal matching pursuit," *IEEE Signal Process. Lett.*, vol. 23, no. 1, pp. 164-168, Jan. 2016.
- [54] D. Declercq and M. Fossorier, "Decoding algorithms for nonbinary LDPC codes over GF(q)," *IEEE Trans. Commun.*, vol. 55, no. 4, pp. 633-643, April 2007.
- [55] C. Poulliat, et al., "Design of regular (2,d/sub c/)-LDPC codes over GF(q) using their binary images," *IEEE Trans. Commun.*, vol. 56, no. 10, pp. 1626-1635, October 2008.
- [56] J. R. Ebert, et al., "On sparse regression LDPC codes," in Proc. IEEE Int. Symp. Inf. Theory (ISIT), Taipei, China, 2023, pp. 2350-2355.
- [57] J. R. Ebert, et al., "Sparse regression LDPC codes," IEEE Trans. Inf. Theory., vol. 71, no. 1, pp. 167-191, Jan. 2025.
- [58] M. Ozates, et al., "An ODMA-based unsourced random access scheme with a multiple antenna receiver," in Proc. IEEE Global Commun. Conf. (GLOBALCOM), Cape Town, South Africa, 2024, pp. 1857-1862.
- [59] H. Jiang et al., "A novel 3D massive MIMO channel model for vehicle-to-vehicle communication environments," *IEEE Trans. Commun.*, vol. 66, no. 1, pp. 79-90, 2018.